# Rapid validation of water wave metamaterials in a desktop-scale wave measurement system ⓕ

Yi Huang ⓘ ; Saishuai Dai ⓘ ; Zhi-Ming Yuan ⓘ ; Laibing Jia ✉ ⓘ

Check for updates

View Online     Export Citation     CrossMark

International Journal of Fluid Engineering 国际流体工程

AIP Publishing

Featured

# Rapid validation of water wave metamaterials in a desktop-scale wave measurement system

View Online   Export Citation   CrossMark

Yi Huang, (ID) Saishuai Dai, (ID) Zhi-Ming Yuan (ID) and Laibing Jia[a] (ID)

**AFFILIATIONS**

Department of Naval Architecture, Ocean and Marine Engineering, University of Strathclyde, 100 Montrose St., Glasgow G4 0LZ, United Kingdom

[a]Author to whom correspondence should be addressed: l.jia@strath.ac.uk

**ABSTRACT**

Metamaterials have a unique ability to manipulate wave phenomena beyond their natural capabilities, and they have shown great promise in electromagnetic and acoustic wave control. However, their exploration in hydrodynamics remains limited. This article introduces a novel desktop-scale wave measurement system, specifically designed for the rapid prototyping and validation of water wave metamaterials. By utilizing 3D printing, the system accelerates the transition from theoretical designs to practical testing, offering a versatile and user-friendly platform. This is further enhanced by a synchronized stereo-camera setup and advanced data processing algorithms, enabling precise measurement and reconstruction of water wave behavior. Our experimental results demonstrate the system's effectiveness in capturing intricate interactions between engineered structures and water waves. This significantly advances rapid prototyping for water wave metamaterial research, underscoring the system's potential to catalyze further innovation in this emerging field.

05 March 2024 12:13:14

## I. INTRODUCTION

Metamaterials are artificially engineered materials that have unique properties not found in nature. The term "metamaterial," originating in the field of optics and derived from the Greek *meta* (meaning "beyond") describes artificial electromagnetic media crafted on a subwavelength scale. These materials are composed of small structure arrays, which endow them with their unique properties. They offer optical qualities that are controllable down to length scales smaller than the wavelength of light and thus are able to make light appear to break conventional rules.

The initial breakthrough in metamaterials was the development of materials with a negative refractive index. In all known natural materials, the incidence of light rays and their refraction are always on opposite sides of the interface's normal line. Their angles from the normal line follow the law of refraction. This means that the indices of refraction for all natural materials are positive. Shelby *et al.*[1] developed a device with square copper split ring resonators and copper wire strips on fiberglass circuit boards. They demonstrated that a microwave beam, when traveling through this engineered material, remained on the same side of the normal line, indicating its capacity

to bend microwaves in the opposite direction compared with natural materials. The material thus has a negative refractive index. This finding demonstrates that engineered materials have the capability to exhibit completely unexpected properties beyond those found in nature.

The capacity of metamaterials to manipulate light propagation opens up numerous applications. One well-known application is cloaking, an invention that can make an object invisible to certain types of detection by redirecting the light around it. Metamaterial structures can direct the pathways of light waves traversing through them. The incident waves are directed to go around an object instead of being scattered. With this technique, the presence of an object can be concealed.[2,3]

Fundamentally, metamaterials are distinguished by their ability to control wave propagation. The fundamental theories for designing optical metamaterials were proposed by Pendry *et al.*[2] and Leonhardt.[4] Pendry *et al.*[2] proposed a theory based on the application of a Galilean coordinate transformation to the Maxwell equations. Leonhardt[4] proposed a theory called "optical conformal mapping" to simplify the anisotropic properties of the designs, leaving only the properties of inhomogeneity.

Both theories provide design methods for the constitutive parameters of the transformation medium, i.e., permittivity and permeability, while keeping the governing equation of the electromagnetic waves unchanged. With appropriately designed medium structures and properties, these constitutive parameters produce localized spatial variations that guide the waves to propagate in a predetermined manner. The wave-ray trajectories travel along a desired path. With their precisely designed shape, geometry, size, orientation, and arrangement, electromagnetic metamaterials are able to perform the functions of blocking, absorbing, amplifying, and bending waves. The development of theories and practical application of optical metamaterials has rapidly attracted widespread attention. According to statistics from the Web of Science Core Collection, the publication rate on the topic of metamaterials has increased rapidly to more than 2700 papers per year.

As far back as 1967, Lighthill[5] created a visual representation, reproduced here as Fig. 1, summarizing his insights into the 26 types of waves that occur in fluids and their interrelationships. These waves found in fluids are depicted within the green-outlined regions of the diagram. The shapes of the areas correspond to the types of wave systems involved. They are also grouped by the characteristics they share. As shown in this plot, both acoustic waves and water waves are members of the family of waves that propagate in fluids.

The concept of manipulating optical waves has inspired research into other families of waves. The design principles of optical metamaterials have been extended to other research fields. Metamaterials with a variety of structures and materials have appeared, and they have been engineered to interact with a variety of waves, such as acoustic waves and water waves.

Metamaterials first appeared in the field of acoustics in 2007, and some hundreds of papers are now published each year on this topic. However, research on water wave metamaterials is still in its early stages. In contrast to electromagnetic waves, which are purely transverse waves, and acoustic waves, which are purely longitudinal waves, water waves involve a combination of both longitudinal and transverse motions. The unique characteristics of water waves thus present a challenge when attempts are made
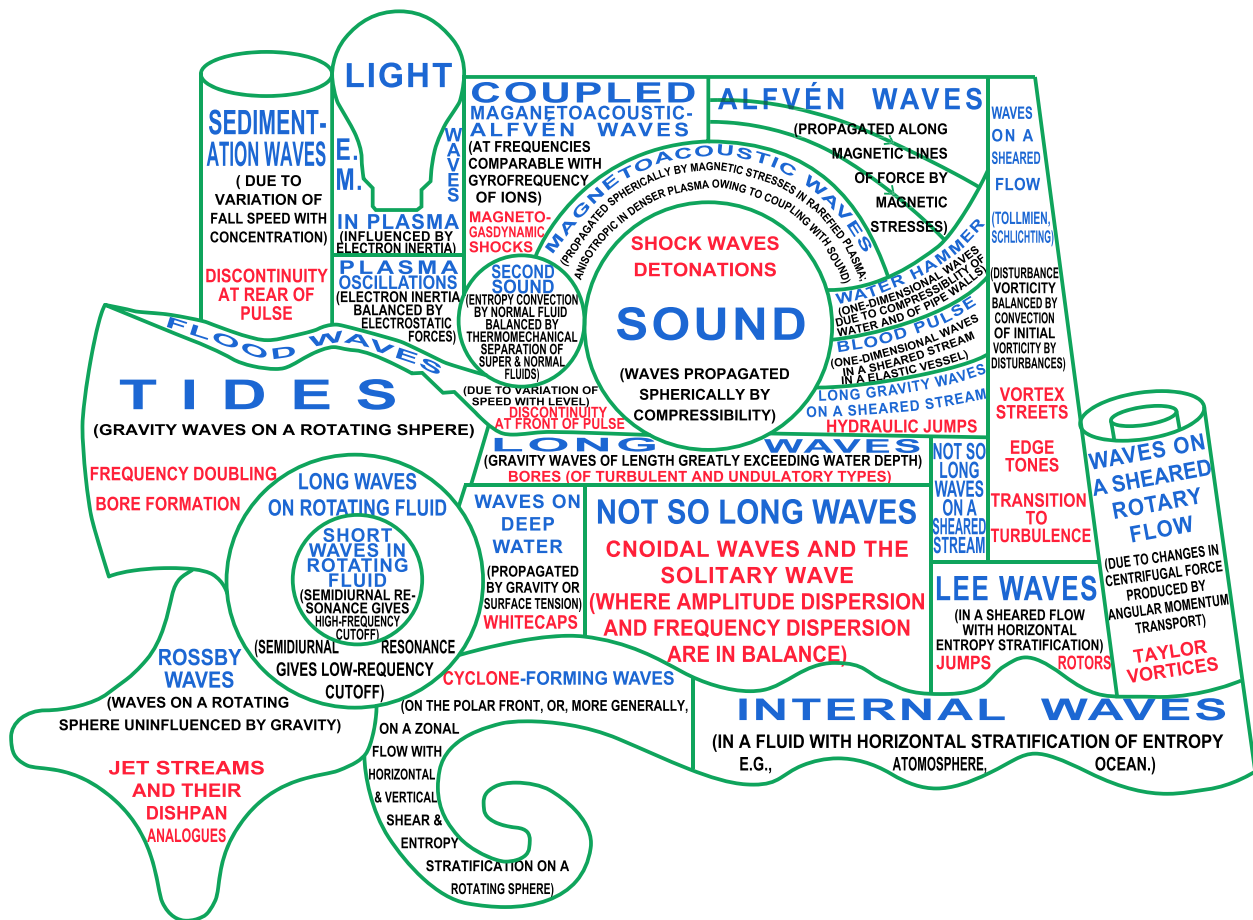


FIG. 1. Waves in fluids. The names of the wave systems are shown in blue. Explanatory remarks for each type of waves are given in black. Key effects of the nonlinear properties of these wave systems are shown in red. Reprinted with permission from M. J. Lighthill, "Waves in fluids," Commun. Pure Appl. Math. **20**, 267–293 (1967). Copyright 1967 Wiley Periodicals, Inc., A Wiley Company.[5]

to apply general design principles to water wave metamaterials. In analogy to the transformations of permittivity and permeability of electromagnetic metamaterials, it is necessary for both the water depth and gravitational acceleration to be spatially varying along the path traveled by the water waves. Altering the gravitational acceleration is not feasible,[6] but researchers in this field have still managed to design metamaterials that can manipulate water waves.

Three ways have been proposed for the design of metamaterials that can control the propagation of water waves. One approach is to use structured bathymetry to control the wave propagation speed and direction. In shallow water, the speed of surface waves can be controlled by varying the seabed topography. Zou et al.[7] found that a gradient depth profile on the bottom of a water channel can achieve broadband cloaking. The structure forms a gradient-index metamaterial. It is a waveguide that converts the incident plane water waves into waveguide-trapped waves. The waves propagate mainly over the waveguide instead of a wider water surface. At the end of the waveguide, the waves are converted back to plane waves again. This cloaking design does not require any structures on the water surface. By repeating this structure with alternating grooves and ridges at the bottom of the water, it is possible to make it work as a reflectionless bent waveguide. Berraquero et al.[8] developed a wave shifter with this kind of metamaterial and demonstrated its efficiency in experiments. Their design of a structured bathymetry with subwavelength rapid abrupt fluctuations in depth shifts the water wave in the direction of the waveguide. A theoretical method based on multiscale homogenization of shallow water theory was developed by Marangos and Porter[9] to find the effective water depth tensor components and predict complex wave propagation characteristics.

Another approach to the design of water wave metamaterials is to control the wave speed using more complex transformation optics principles. Such metamaterials look more like the designs for electromagnetic waves, because they implement similar design principles. Zareei and Alam[6] proposed a design that requires only a change in water depth to achieve a nonlinear transformation for water waves. Their theoretical approach connects transformation optics and shallow-water waves. Farhat et al.[10] proposed a structured metamaterial to generate artificial anisotropic properties in a fluid. Their theoretical model based on homogenization theory was successfully tested by comparison with numerical simulations and experiments for an example of water wave cloaking. Iida and Kashiwagi[11] proposed another theoretical approach to the design of shallow water wave metamaterials based on an analogy between waves in a water channel and in an electric circuit. Their anisotropic network model provides another explanation for the success of the design of Farhat et al.[10] for cloaking a cylinder. Using a conformal mapping, Dupont et al.[12] proposed another method for constructing metamaterials that can cloak a cylinder in water waves. As the cylinder is cloaked from the water waves, the drift force to which the cylinder is subjected is reduced. Park et al.[13] proposed a metamaterial cloak based on the idea of guiding viscous forces and used coordinate transformation of fluidic space to study the viscous forces in the flow around a cylinder. They demonstrated that their cloaking metamaterial could achieve a drag-free state through anisotropic mapping of viscosity.

A third approach to developing water wave metamaterials is through a scattering cancellation method. Wave interference is used here, instead of changing the water depth as employed in the first two approaches. Given that variations in water depth in deep water have minimal impact on the propagation of water waves, this technique is essential for developing water wave metamaterials for ocean engineering applications. Newman[14] found that placing multiple cylinders in a circle can cloak another cylinder located at the center of this circle. Zhang et al.[15] demonstrated that as few as eight cylinders can manipulate the scattered waves to achieve wave concentration and invisibility effects for water waves. Using elastic plate rings floating on the water surface around a cylinder, Iida et al.[16] demonstrated how to cloak a bottom-mounted cylinder against water waves. Their cloaking structure is constructed from four or more concentric rings and has an outer diameter greater than three times that of the cylinder. The wave drift force almost vanishes for an appropriate rigidity of the rings. Han et al.[17] found that a one-dimensional groove array can direct water waves into one direction by exciting unidirectional surface polaritons on the water surface. Porter[18] explored a metamaterial design using thin parallel plates reaching above the water surface. The channels between the plates form a waveguide that confines water waves. They found that this plate array can act as a perfectly transmitting negative-refraction metamaterial. Li et al.[19] combined this kind of plate waveguide with the first approach of depth-profiled bathymetry to develop annular concentrators that can manipulate water waves with wave concentration and invisibility effects.

On the basis of all three approaches described above, water metamaterials have been designed and have shown their capabilities in controlling water waves. They have been used in water wave cloaking, drag reduction, and wave scattering. They provide the foundation for a variety of applications, such as protection of harbors and coastal assets, and ocean wave energy harvesting on harsh surfaces and in underwater environments. Some other techniques for wave manipulation, such as the wave-passing effect observed in the formation swimming of ducklings[20] may also be incorporated into the design of metamaterials in the future.

In existing metamaterial studies, the focus has mainly been on the design of water wave metamaterials. The experimental validations have been mainly based on the optical shadowing technique, a method that projects light into the water and records changes in brightness caused by the curvature of the water surface. This method can provide qualitative results about wave propagation but cannot measure the absolute wave height in experiments. Another method uses multiple wave probes in a wave tank to measure the wave heights at limited positions.

Unlike previous methods that have primarily focused on theoretical or computational models, our work introduces a novel, comprehensive approach that seamlessly integrates rapid prototyping and experimental testing. Central to this innovation is the adoption of an advanced in-lab optical measurement technique. This method offers high spatial resolution, enabling precise measurement of absolute wave heights across the entire water surface, overcoming the limitations of shadowing and point measurements. This enhancement in precision and scope is a considerable step forward from conventional practices and can be extended to wave measurements in field tests.

Further distinguishing our approach is the strategic incorporation of 3D printing technology. This integration revolutionizes the prototyping process, accelerating the creation and modification of metamaterial designs. The agility provided by this technology substantially increases the efficiency and adaptability of our research process. Additionally, the compact nature of our experimental setup is instrumental in facilitating rapid concept validation. This scaled-down model not only streamlines the research process, but also enables faster progression from theoretical constructs to practical testing. These collective innovations open up exciting new possibilities for the exploration and application of these structures in the dynamic field of water wave manipulation and in the application of metamaterials.

In this article, we introduce our water wave metamaterial validation system that can quickly validate the designs of metamaterials with experiments. The remainder of the article is organized as follows: Sec. II describes the methodology of our study, Sec. III presents our experimental results, and Sec. IV concludes our study of the desktop-scale wave measurement system and its use in rapid validation of water wave metamaterials.

## II. EXPERIMENTAL SETUP AND DATA PROCESSING

The desktop water wave metamaterial validation system includes both an experimental setup and data processing. The experimental setup allows for the quick fabrication of water wave metamaterials and testing of their performance in waves, while the data processing provides precise results from the experimental data. The combination of these two components makes it possible to rapidly test and refine these designs of water wave metamaterials, ensuring that they are effective and efficient in water wave manipulation.

In our study, a fused deposition modeling (FDM) 3D printer is used to build the prototypes of water wave metamaterials. Given that the water wavelengths are much longer than the printer's resolution, the precision of an FDM printer suffices for manufacturing prototype models. The models are then placed in a water tank as shown in Fig. 2 for wave making and measurement. The desktop-scale wave maker and wave tank, including the other equipment and apparatus used in this study, are placed in a dedicated section inside the Kelvin Hydrodynamic Laboratory at the University of Strathclyde.
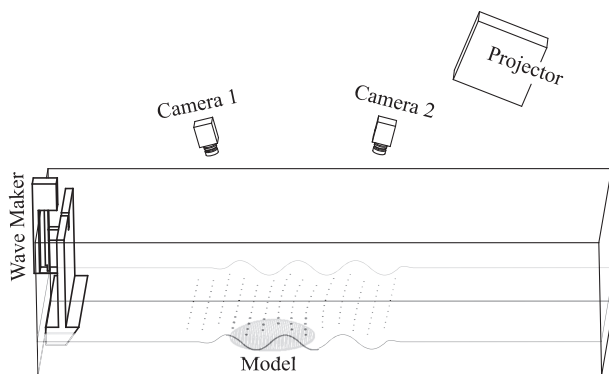
## A. Experimental setup

The water tank is made of glass with dimensions suitable for a desktop: $1500 \times 680 \times 300 \text{ mm}^3$ in length, width, and height, respectively. A plunger-type wavemaker is located at the left side of the tank. The wavemaker is driven by a stepper motor (NEMA23, maximum torque 2.0 N m). The motion of the plunger is directly controlled by an Arduino Nano 33BLE board. A projector (XGIMI Elfin) with a native resolution of $1280 \times 720$ pixels hangs over the tank to project certain patterns on the water surface. The water surface is seeded with hollow microsphere glass bubbles (3M K20). These microbubbles have an average diameter of 60 $\mu$m and a density of 0.20 g/cm$^3$. They float on the water surface to enhance its reflective properties. Patterns projected onto the water surface are captured by two global-shutter industrial cameras (Daheng Mercury2 USB 3.0) at a frame rate of 100 fps, with a resolution of $1536 \times 2048$ pixels. These cameras are controlled by MATLAB and synchronized using an additional Arduino Nano board. In our desktop tank, no wave absorber module is placed at the right end of the tank.

## B. Fast prototyping system

An integral component of our experiment apparatus is the FDM 3D printer (Anycubic Kobra Plus). It allows us to quickly bring designed models into a physical model for testing, facilitating a hands-on iterative development cycle that involves fabrication. In the prototyping of metamaterial structures, our setup shortens the iteration window from the weeks required by conventional techniques, even with experienced technicians, to just hours.

This rapid prototyping system significantly streamlines the metamaterial development process. It enables us to quickly evaluate the hydrodynamic responses of different designs without the lengthy lead times typically associated with traditional manufacturing methods. This agility is vital for testing multiple design iterations and for studying the effects of subtle geometric changes on the wave manipulation capabilities of the metamaterials.

Moreover, the use of 3D printing opens up the possibility of exploring complex structures that would be challenging, if not impossible, to fabricate using conventional methods. This feature is particularly beneficial for testing theoretical models that require precise geometrical features at a scale that traditional tools cannot achieve. Consequently, the fast prototyping capability has become an indispensable tool in our metamaterial design and testing workflow, fostering innovation and enabling a deeper understanding of the interaction between water waves and metamaterial structures.

## C. Experimental procedure

In our study, we adopt the following procedure to carry out experiments.

The first step is to place every device in position. The projector may leave a bright reflection of its lens on the water surface. The positions of the two cameras need to be carefully adjusted to avoid capturing the reflection of the lens in the main measurement regions.



**FIG. 2.** Experimental setup.

05 March 2024 12:13:14

Simultaneously, the distance between the two cameras needs to be sufficiently large to increase the accuracy of the triangulation measurement. Increasing the depth of field by reducing the lens aperture or using tilt–shift lenses can further improve the performance of the system.

The second step is to calibrate the cameras in the measurement system. In this step, the intrinsic and extrinsic parameters of the cameras are calculated from multiple photographs of a checkerboard captured by both cameras. The intrinsic parameters of a camera refer to its internal characteristics, such as focal length and lens distortion. The extrinsic parameters refer to the relative position and orientation of the two cameras in relation to each other. They are essential in determining the 3D coordinates of the water surface.

In this step, a $12 \times 9$ aluminum checkerboard made of 15 mm squares is used as the calibration target to calibrate the cameras. Our early trials used a checkerboard printed on a piece of paper, which was then pasted onto a smooth solid surface (a wooden or acrylic board). However, unevenness of the surface caused by unevenly applied glue and upturning of the paper resulting from the humidity in the tank area introduced additional systematic errors into the calibration process. We found that an aluminum checkerboard with an antireflection coating worked much better as a calibration target compared with a paper checkerboard. The improved calibration target significantly reduced the average calibration error from 0.5–0.7 to 0.1–0.15 pixels. During the calibration process, the checkerboard needs to cover the whole testing region. At the same time, the checkerboard is rotated to different angles to enhance the rigidity of the calibration. Both procedures are used to ensure that the cameras' parameters can be accurately calculated.

The third step is to validate the precision of the setup by capturing a two-level 3D calibration plate from LaVision and the still water surface. This plate, typically used for calibrating LaVision's stereo-camera systems, has proved ideal for our purposes in assessing the absolute precision of our stereo-camera system. The measurement confirms the vertical resolution and provides a measure of the system's accuracy. In the measurement of the still water surface, the water remains calm, creating a perfectly flat surface. Consequently, the reconstructed water surface should be flat too. The result is used to build a horizontal reference level for the wave measurements.

In computer vision, especially when it comes to triangulation, a checkerboard is the default choice of patterns. In addition to using it in calibration, we have also conducted several trial runs using projected checkerboard patterns of various sizes for either still or wave reconstruction. The trial results suggest that checkerboard patterns are highly accurate while requiring only a single line of code for the reconstruction process (in MATLAB). The checkerboard detection function in MATLAB requires a significant amount of computing time. As a result, we have to either reduce the grid size to a low double-digit number, which results in lower resolution in the final reconstruction, or endure a long computation time of around one hour per frame, neither of which is optimal.

Thus, we have selected the dotted grid as the projection pattern, where the product of the number of rows and columns must be odd to ensure correct numbering (also required when using a checkerboard). The dotted grid is structurally more straightforward

to identify than the checkerboard, and the regular spacing of dots allows for easy detection and accurate measurement of the water surface elevation.

In this step, the measurement region is also identified with the photographs taken by two cameras. Image masks are generated to filter out those areas without useful information. We use 500 frames of the still surface to estimate the error of the reconstruction algorithm, which will be discussed in further detail in Sec. III.

The fourth step is to put a metamaterial model in water, fixed at the bottom of the tank. We use the wavemaker to generate certain frequencies and amplitudes of waves to test the performance of the metamaterial design. In our tests, we repeat each parameter set five times to ensure the repeatability of the system.

For wave generation, we selected the amplitude and frequency based on the requirement of shallow water waves, the capability of the stepper motors, and the visibility of the wave–structure interactions. The torque of the step motors determines the maximum frequency and amplitude of the waves we can generate. A NEMA23 stepper motor at a maximum torque of 0.6 N m moves the paddle at a pace of 2 Hz at 1 mm amplitude, or a higher amplitude at a lower frequency. A NEMA23 stepper motor at a maximum torque of 2.0 N m is capable of generating waves up to 3 mm amplitude at a frequency equal to or below 2 Hz. To ensure both accuracy and consistency, active feedback has also been enabled with the motor's motion control.

The wave-making script is written using the Arduino IDE. Since the built-in Arduino stepper motor library supports only linear acceleration, we have developed a custom motion script using the tone function. This function on the Arduino board generates a square wave of the specified frequency, which is then used to generate the steps of our sinusoidal velocity profile.

For instance, to control the plunger moving with an amplitude $A$ at a frequency $f$, we can calculate the tone frequency as follows:

$$f_{tone} = 2\pi A f \frac{P}{S} \sin(2\pi f t), \tag{1}$$

where $P$ is the number of microstep counts per rotation for the stepper motor, $S$ is the step length for the rail, and $t$ is time. It is also noticed that the traveling distance of the paddle does not directly translate to wave amplitude. In our study, the water wave heights are around half of the paddle's traveling distance, depending on the water depth.

We tested wave absorption with a beach made of plastic sheets. The results showed that for a desktop-scale water tank, the wave absorber could cancel the reflective wave effectively, resulting in standing waves propagating in the tank. Additionally, the absorber also occupied valuable space in the tank. Thus, we decided to take the beach out, extending the wave travel length by another 30 cm, and to generate a limited number of waves at each testing session. We disregard the effect of wave reflection, since image capture occurs before the waves reach the tank's glass end wall.

Image data captured by the stereo cameras is transferred to the system RAM first, instead of being written directly to hard drives, to ensure accurate time steps between frames, with the side benefit of ensuring synchronization of the two cameras.

05 March 2024 12:13:14

## D. Data processing

The data processing procedure consists of four main steps:

1. Calibrating the cameras by calculating their intrinsic and extrinsic parameters.
2. Reconstructing the still water surface.
3. Reconstructing the water surface with waves.
4. Repeating each frequency and amplitude set five times to minimize uncertainty.

For camera calibration, we use the built-in stereo camera calibrator in the MATLAB image processing and computer vision toolbox, along with 50 pairs of images. As mentioned above, the software has reported an average error of 0.1–0.15 pixels. The calculated camera parameters are stored as a calibration session. It will be used for a prolonged period of time, typically a month or so, provided that the camera position remains unchanged throughout the experiment.

Although MATLAB has built-in functions for checkerboard reconstruction, the process is very slow. In our study, we create multiple self-defined functions to process the dotted grid, and these perform significantly faster than MATLAB's built-in functions for image processing.

For reconstruction, we first need to undistort the still water surface images using the camera parameters from the calibration process, and then pass the images through a custom function to locate their corners. With the corners' location and an offset of a safety margin, we create masks for each camera to reduce the image file size to only the region of interest.

The reconstruction algorithm includes locating each dot's center in the image. We use the MATLAB function "findcircle" to identify them. The built-in triangulate function is used to calculate the coordinates of grid points on the wave surface.

## III. RESULTS

The following results have been obtained using the fast prototyping and wave measurement system.

## A. Precision in surface measurement

The two-level calibration plate (LaVision, 106-10-2) used to measure the absolute precision of the system was manufactured using Computer Numerical Control (CNC) from a single aluminum
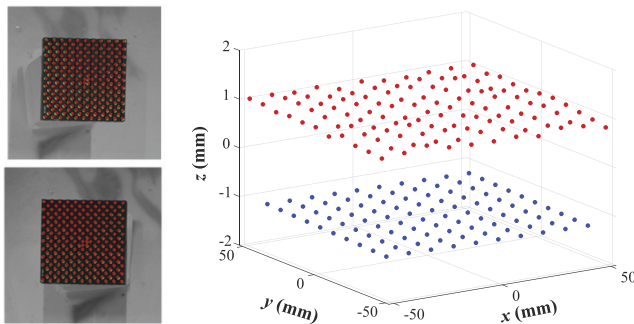


**FIG. 3.** Two-level plate recognition and reconstruction based on averaging 500 frames of data.
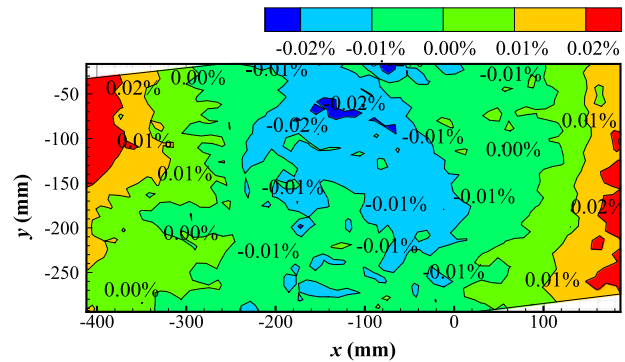


**FIG. 4.** Relative error of the reconstructed still water surface.

block. It is $106 \times 106$ mm$^2$, with 223 recognizable markers with a uniform diameter of 2.2 mm and a distance of 10 mm between markers. The plate has two flat levels with a vertical gap of 2 mm in height. These tests validate the vertical resolution and provide a measure of the system's accuracy.

The two panels on the left of Fig. 3 present the recognition results from one pair of stereo-camera frames. These results from the LaVision calibration plate are essential for ensuring that the stereo-camera system accurately identifies reference points across planes at two different height levels. The plot on the right of Fig. 3 shows the average results of the 3D reconstruction based on 500 frames of data captured at a distance of 2.1 m from the $106 \times 106$ mm$^2$ plate. The gap between two reconstructed planes is 2.099 mm. The absolute error in the measurement is 0.099 mm. The level of uncertainty is in line with conventional wave measurement systems using resistance wave probes.

Before capturing and reconstructing waves, we also test the performance of the algorithm and equipment by reconstructing a still water surface. Thus, a sample set consisting of 500 frames of still water is used to establish a benchmark for error.

Figure 4 shows the relative error of the reconstructed water surface normalized by the distance between the cameras and the water surface. The relative error is sufficiently small, at a maximum of $\sim\pm0.02\%$. The surface mean roughness is 0.20, and the effective surface mean curvature is 0. Although the maximum error appears at the top left and bottom right corners, its value is very small, at a level of 0.02% in relative error. The result gives a good depiction of the flatness of the still water surface.

These measurements of the two-level calibration plate and still water surface provide sufficient confidence in the stereo-camera setup to continue to the next phase of the experiment.

## B. Case I: Reconstruction of a single wave propagation

A typical metamaterial design is selected to test our rapid validation approach for metamaterials using our desktop-scale wave measurement system. The structure is shown in Fig. 5(a). It is a channeled spherical cut with a radius of 90 mm and a height of 35 mm, and each channel is 5 mm wide.

For metamaterials, the spherical cut is a simply and effective structure, especially in the case of electromagnetic and acoustic waves, when it appears in the form of various alternating Lueb-
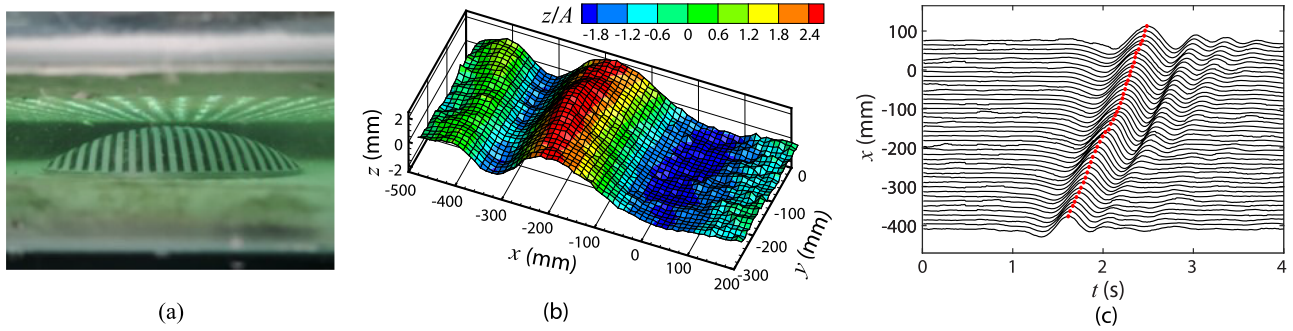
**FIG. 5.** (a) Fabricated channeled spherical cut metamaterial. (b) Snapshot of reconstructed water surface under a single 2 Hz wave at 2.0 s. (c) Time history of wave elevations along the centerline in the $y$ direction.

urg lens designs. The channeled spherical cut design that we have selected here is a combination of both the lossless wave bent channel proposed by Berraquero et al.[8] and the plate array design proposed by Porter.[18] The metamaterial is placed in the tank, leaving enough

space for the wave to propagate and settle. The exact location of the structure, shown in Fig. 6, is $x = -224.1$ mm, $y = -196.7$ mm.

The purpose of this test is to study the transient response of the wave to a metamaterial structure by measuring the wave evolution
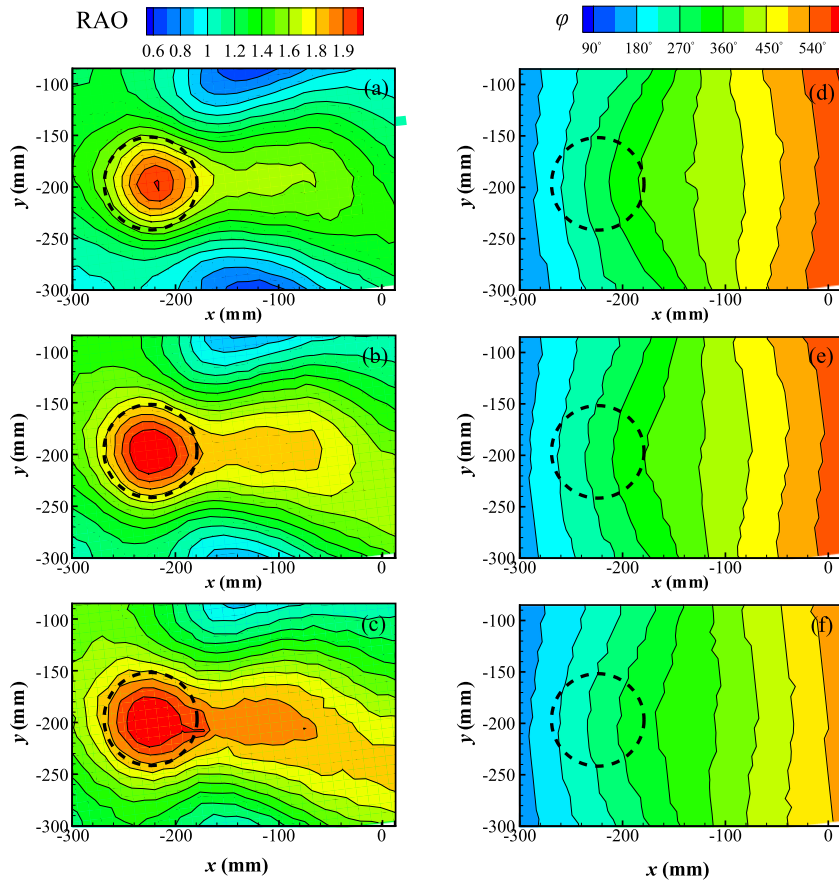


**FIG. 6.** Response amplitude operator (RAO) for different water depths along with the corresponding wave phase contours: (a) and (d) 37 mm; (b) and (e) 43 mm; (c) and (f) 47 mm. The position of the metamaterial structure is indicated by the dashed circles.

over time. The structure is tested with waves at a frequency of 2.0 Hz and an amplitude of 1.49 mm. The desktop flume water depth is set to 40.0 mm.

Figure 5(b) shows the reconstructed water surface. It is the instantaneous water surface at time 2.0 s, when the wave reaches the region with the submerged metamaterial structure. In this study, we operate the plunger for only one cycle, generating only one period of a wave. On the figure, the highest place is marked as red. Its position is over the top of the center of the channeled spherical cut. This is caused by the sloshing effect, due to the decrease in water depth resulting from the presence of the spherical cut.

As the snapshot of the water wave surface cannot reveal the evolution of the wave, the wave surface is sliced with a cut in its center. Figure 5(c) shows the result of one row (the 15th) of the 35 rows with its 60 points and plots the time history of the elevation at each point. The wave elevation is amplified for a clear view of the wave propagation. The lower part of this plot is the region preceding the metamaterial structure, the middle part is the place where the channeled spherical cut is located, and the upper part shows the wave propagation after encountering the spherical cut. The red dots mark the peak of the wavefront at different positions along the centerline. The dots in the lower part of the plot show linear trends as time advances, and then a bend appears, followed by a recovery to a linear trend later in time. The change at the center results from the presence of the metamaterial structure. As the wave interacts with the structure, the dramatically increasing and decreasing water depth in the metamaterial region leads to a sudden decrease in the wave velocity at around 2.0 s, which is also the time shown in Fig. 5(b) as a demonstration of instantaneous water surface reconstruction where the peak of the wave surface coincides with the location of the top of the metamaterial.

In Fig. 5(c), the phenomenon of wave dispersion can be observed within the test region. The input wave, conforming to shallow water wave conditions, exhibits distinct characteristics before and after encountering the metamaterial structure. Initially, in the region before the metamaterial structure, the wave exhibit minimal dispersion, as is evident from the appearance of only one peak. This part of the wave's journey is characterized by relatively stable propagation, consistent with expectations in a linear, undisturbed wave environment.

However, upon the wave's interaction with the metamaterial structure, a significant transformation in its is noted. After this interaction, there is a marked emergence of obvious wave troughs and peaks, indicative of pronounced wave dispersion. This change is a clear departure from the previously observed linear wave conditions, highlighting the metamaterial's influential role in altering wave dynamics.

## C. Case II: Reconstruction of waves for different water depths

In this case study, we further examine the performance of the structure under the same wave parameters that were used in case I, but for different depths of the water in the tank. The aim in this case is to analyze the amplitude and phase responses of waves interacting with a metamaterial structure.

The results, shown in Fig. 6, offer a comprehensive illustration of how the subaquatic metamaterial structure influences water

waves for different water depths. Specifically, Figs. 6(a)–6(c) provide a detailed representation of the response amplitude operator (RAO) of water waves for three different water depths: 37, 43, and 47 mm. Figures 6(d)–6(f) show the phase plots of waves that pass the structure.

For all these different depths, a notable concentration of elevated water levels can be observed in close proximity to the pinnacle of the submerged metamaterial structure. This concentration phenomenon is most conspicuous for the greatest depth of 47 mm, where a substantial and localized increase in elevation is particularly pronounced in comparison with the initial wave excitation. As the water depth increases, the concentration effect remains centered around the apex of the underwater metamaterial.

Furthermore, alongside this concentration around the structure, there is an observable "cliff" of high-RAO regions, which becomes more prominent and widens as the water depth increases. Simultaneously, the water surface exhibits areas of low RAO, depicted as a spectrum ranging from light to dark blue in Figs. 6(a)–6(c), attributable to the conservation of energy carried by the water waves.

Considering potential applications in ocean engineering, it is worth noting that the regions of high RAO created by the metamaterial could serve as an ideal location for deploying wave energy converters. This strategic placement has the potential to significantly enhance the energy output, while the areas of low RAO could be used for protection from damage by large waves, offering shelters for valuable assets within the marine environment.

Figures 6(d)–6(f) present the wave phase contours $\phi$ for different water depths. The lines in the plots represent the motion of the wave front during its traverse across the tank. Initially, as the wave originates from the wavemaker, it is a straight line. As it approaches the metamaterial structure, as shown on the left-hand side of each plot, the metamaterial starts to alter the propagation of the water wave. Upon entering the metamaterial region, the wave front forms a bow-shaped distribution, which is a consequence of the gradual reduction in velocity resulting from the diminishing water depth induced by the metamaterial. Subsequently, as the wave progresses across the metamaterial zone, it gradually regains its original configuration, returning to a straight and uniform propagation pattern.

In Fig. 6(d), for a depth of 37 mm, the contours densely populate the diagram, indicating a rapid phase change. Conversely, for the deepest water depth of 43 mm as shown in Fig. 6(f), the contours adopt a smoother and more widely dispersed appearance. The difference in the gaps between lines is the result of different wave travel speeds, which correspond to the differences in water depth.

These results serve to demonstrate the ability of the metamaterial to alter and control the elevation and phase of water waves. They also provide empirical evidence that the metamaterial's effectiveness is influenced by the depth of the water.

## IV. CONCLUSION

This study presents a novel approach to the rapid validation of water wave metamaterials using a desktop-scale wave measurement system. Our experimental setup and data processing techniques provide a unique platform for the efficient prototyping, testing, and analysis of water wave metamaterial designs. The integration of a 3D

printing system for rapid prototyping, along with advanced stereo-camera setups and data processing algorithms, has demonstrated a significant advancement in the field of hydrodynamic metamaterial research.

Our findings indicate that not only is the system capable of accurately capturing complex interactions between water waves and engineered structures, but it also offers insights into the potential for modifying wave behavior with different metamaterial designs. The experimental results confirm the system's effectiveness in manipulating wave propagation, highlighting its potential in various practical applications, including coastal protection, wave energy harvesting, and marine engineering.

The versatility and user-friendliness of the system underscore its potential as a valuable tool for researchers and engineers. By enabling rapid iteration from theoretical designs to practical testing, the system significantly reduces the development time and cost associated with experimental water wave metamaterial research.

While our study focuses on specific metamaterial designs, the methodology and system developed here are adaptable and can be extended to a broader range of hydrodynamic applications. Future research should aim to explore these potential applications, as well as further refining the system for enhanced accuracy and efficiency.

In conclusion, the desktop-scale wave measurement system introduced in this study marks a pivotal step toward the rapid and efficient development of water wave metamaterials, paving the way for novel solutions in controlling and utilizing water waves.

## AUTHOR DECLARATIONS

### Conflict of Interest

The authors have no conflicts to disclose.

### Author Contributions

**Yi Huang**: Data curation (equal); Formal analysis (equal); Investigation (equal); Methodology (equal); Validation (equal); Visualization (equal); Writing – original draft (equal); Writing – review & editing (equal). **Saishuai Dai**: Resources (equal); Supervision (equal). **Zhi-Ming Yuan**: Formal analysis (equal); Resources (equal); Writing – review & editing (equal). **Laibing Jia**: Conceptualization (equal); Formal analysis (equal); Funding acquisition (equal); Investigation (equal); Methodology (equal); Project administration (equal); Supervision (equal); Visualization (equal); Writing – original draft (equal); Writing – review & editing (equal).

## DATA AVAILABILITY

The data that support the findings of this study are available from the corresponding author upon reasonable request.

## REFERENCES

[1] R. A. Shelby, D. R. Smith, and S. Schultz, "Experimental verification of a negative index of refraction," Science **292**, 77–79 (2001).

[2] J. B. Pendry, D. Schurig, and D. R. Smith, "Controlling electromagnetic fields," Science **312**, 1780–1782 (2006).

[3] D. Schurig, J. J. Mock, B. Justice, S. A. Cummer, J. B. Pendry, A. F. Starr, and D. R. Smith, "Metamaterial electromagnetic cloak at microwave frequencies," Science **314**, 977–980 (2006).

[4] U. Leonhardt, "Optical conformal mapping," Science **312**, 1777–1780 (2006).

[5] M. J. Lighthill, "Waves in fluids," Commun. Pure Appl. Math. **20**, 267–293 (1967).

[6] A. Zareei and M.-R. Alam, "Cloaking in shallow-water waves via nonlinear medium transformation," J. Fluid Mech. **778**, 273–287 (2015).

[7] S. Zou, Y. Xu, R. Zatianina, C. Li, X. Liang, L. Zhu, Y. Zhang, G. Liu, Q. H. Liu, H. Chen, and Z. Wang, "Broadband waveguide cloak for water waves," Phys. Rev. Lett. **123**, 074501 (2019).

[8] C. Berraquero, A. Maurel, P. Petitjeans, and V. Pagneux, "Experimental realization of a water-wave metamaterial shifter," Phys. Rev. E **88**, 051002 (2013).

[9] C. Marangos and R. Porter, "Shallow water theory for structured bathymetry," Proc. R. Soc. A **477**, 20210421 (2021).

[10] M. Farhat, S. Enoch, S. Guenneau, and A. Movchan, "Broadband cylindrical acoustic cloak for linear surface waves in a fluid," Phys. Rev. Lett. **101**, 134501 (2008).

[11] T. Iida and M. Kashiwagi, "Small water channel network for designing wave fields in shallow water," J. Fluid Mech. **849**, 90–110 (2018).

[12] G. Dupont, S. Guenneau, O. Kimmoun, B. Molin, and S. Enoch, "Cloaking a vertical cylinder via homogenization in the mild-slope equation," J. Fluid Mech. **796**, R1 (2016).

[13] J. Park, J. R. Youn, and Y. S. Song, "Hydrodynamic metamaterial cloak for drag-free flow," Phys. Rev. Lett. **123**, 074502 (2019).

[14] J. Newman, "Cloaking a circular cylinder in water waves," Eur. J. Mech., B: Fluids **47**, 145–150 (2014).

[15] Z. Zhang, S. Liu, Z. Luan, Z. Wang, and G. He, "Invisibility concentrator for water waves," Phys. Fluids **32**, 081701 (2020).

[16] T. Iida, A. Zareei, and M.-R. Alam, "Water wave cloaking using a floating composite plate," J. Fluid Mech. **954**, A4 (2023).

[17] L. Han, S. Chen, and H. Chen, "Water wave polaritons," Phys. Rev. Lett. **128**, 204501 (2022).

[18] R. Porter, "Plate arrays as a perfectly-transmitting negative-refraction metamaterial," Wave Motion **100**, 102673 (2021).

[19] C. Li, L. Xu, L. Zhu, S. Zou, Q. H. Liu, Z. Wang, and H. Chen, "Concentrators for water waves," Phys. Rev. Lett. **121**, 104501 (2018).

[20] Z.-M. Yuan, M. Chen, L. Jia, C. Ji, and A. Incecik, "Wave-riding and wave-passing by ducklings in formation swimming," J. Fluid Mech. **928**, R2 (2021).